

NBSIR 73-349

CHARACTERIZATION OF A SUPERCONDUCTING COIL COMPOSITE

C. W. Fowlkes
P. E. Angerhofer
R. N. Newton
A. F. Clark

Cryogenics Division
Institute for Basic Standards
National Bureau of Standards
Boulder, Colorado 80302

Interim Report

December 1973

Prepared for:
Annapolis Laboratory
Naval Ship Research and Development Center
Annapolis, Maryland 21402



NBSIR 73-349

CHARACTERIZATION OF A SUPERCONDUCTING COIL COMPOSITE

C. W. Fowlkes
P. E. Angerhofer
R. N. Newton
A. F. Clark

Cryogenics Division
Institute for Basic Standards
National Bureau of Standards
Boulder, Colorado 80302

Interim Report

December 1973

Prepared for:
Annapolis Laboratory
Naval Ship Research and Development Center
Annapolis, Maryland 21402



U.S. DEPARTMENT OF COMMERCE, Frederick B. Dent, Secretary

NATIONAL BUREAU OF STANDARDS Richard W. Roberts, Director

TABLE OF CONTENTS

		Page
	ABSTRACT	1
1.	INTRODUCTION	1
2.	MACROSCOPIC MATERIAL PROPERTIES	5
	2.1 Simplified Material Properties	5
3.	MICROMECHANICAL ANALYSIS	8
	3.1 Volume-Fraction Determination	9
	3.2 Predictive Laws	13
4.	SPECIMENS	18
5.	THERMAL EXPANSION	22
	5.1 Procedure	22
	5.2 Data	25
	5.3 Discussion	29
6.	YOUNG'S MODULI AND POISSON'S RATIOS	29
	6.1 Procedure	29
	6.2 Data	36
	6.3 Discussion	36
7.	PREDICTED VERSUS MEASURED PROPERTIES	40
	7.1 Preliminary Coil Values	42
	7.2 Effect of Curvature	44
8.	CONCLUSIONS	44
9.	ACKNOWLEDGEMENTS	45
	REFERENCES	46

LIST OF FIGURES

		Page
Figure 1.	Cross section of the superconducting coil tested	3
Figure 2.	Schematic of superconducting solenoid coil showing construction and coordinate axes	4
Figure 3.	Average spacing of coil composite wires	12
Figure 4.	Two simple micromechanical models of a composite material	14
Figure 5.	Schematic of specimen structures and orientations (a) Longitudinal specimen (b) Radial or transverse specimen	19
Figure 6.	Schematic of thermal expansion apparatus	23
Figure 7.	Thermal expansion (a) and tensile (b) specimens	24
Figure 8.	Thermal contraction of superconducting coil materials .	27
Figure 9.	Thermal expansion coefficient of superconducting coil materials	28
Figure 10.	Strain gage location on tensile specimens	30
Figure 11.	Tensile test apparatus	32
Figure 12.	Schematic of gage circuit	33
Figure 13.	Typical apparent stress strain curve	34
Figure 14.	Young's modulus versus temperature for superconducting coil materials	38
Figure 15.	Poisson's ratio versus temperature for superconducting coil materials	39

LIST OF TABLES

Table 1.	Room-temperature constituent material properties for micromechanics calculations.	10
Table 2.	Equivalent volume fractions for transverse directions. .	11
Table 3.	Elementary micromechanics equations for predicting composite properties	16
Table 4.	Thermal contraction and coefficient of thermal expansion for superconducting coil materials	26
Table 5.	Young's moduli and Poisson's ratio for superconducting coil materials	37
Table 6.	Room-temperature properties of the superconducting coil composite, calculated values and measured values. .	41

CHARACTERIZATION OF A SUPERCONDUCTING COIL COMPOSITE

C. W. Fowlkes, P. E. Angerhofer, R. N. Newton, and A. F. Clark

The superconducting coil composite material utilized by the Annapolis Laboratory of the Naval Ship Research and Development Center is characterized by its mechanical and thermal properties. The Young's moduli, Poisson's ratios, and thermal contractions are measured from room temperature to 4 K and presented in this interim report. A micromechanical analysis based upon volume fractions of constituents is used to predict room-temperature properties, and a comparison is made to the measured values.

1. INTRODUCTION

Operating conditions of superconducting motors or generators include a very wide range of temperatures and mechanical stresses and high magnetic fields. These complex and extreme environments add to the designer's problem of determining reliability and establishing realistic margins of safety. A particularly difficult problem is the requirement of long life under fatigue conditions. The coil-design process must include prediction of electrical or magnetic performance, heat transfer characteristics, and structural reliability. Analyses of structural reliability of the coil depends on many construction variables and is hampered by lack of knowledge of mechanical and thermal properties of the coil composite. The level of investment in this type of equipment dictates a need for more refined and accurate analyses.

Stress analysis of the coil structure in a superconducting motor must consider (a) residual stresses due to winding and potting, (b) stresses due to mechanical interaction of the coil structure with adjacent parts of the machine and its support, (c) stresses within the composite winding structure due to differential thermal contraction during cool-down and (d) stresses due to magnetic forces.

The analyses of such a structure may be conveniently and clearly divided into two different areas: macromechanical and micromechanical. Macromechanical analysis treats the composite coil structure as a homogeneous material characterized by anisotropic material properties.[1,2,3,4] This is a practical approach for a wide variety of engineering design problems provided that the anisotropic material properties can be characterized accurately. Micromechanical analysis focuses on the coil properties on a much finer scale, giving detailed consideration to the stress distribution around superconducting wires embedded in an epoxy matrix, each characterized by different sets of material properties. Micromechanical analysis can be used to estimate the anisotropic moduli required for macroscopic analysis. Conversely, given a regional (average) stress calculated from macromechanical analysis, localized stresses in the epoxy and wires may be calculated using micromechanics.

A great body of literature has been developed within the last decade on micromechanical analysis of composite materials, particularly with reference to fiber-reinforced plastics (fiberglass, etc.). Studies of these materials rely greatly on powerful finite-element mathematical techniques for stress analysis,[5,6] which have been developed extensively in the last decade, where continuum analytical techniques are intractable. Portions of this literature are applicable to the superconducting coil analyses, and implicit reference to the composite materials literature must be recognized throughout this work.

This interim report focuses on the structural analysis of a particular coil built at NSRDC. Measured materials property data such as Young's modulus, Poisson's ratio, and thermal expansion, which are required input to the coil design, are presented. A cross section and schematic of the coil studied in this paper are shown in Figures 1 and 2. The test results presented in this paper represent a first step toward establishing a data base of material properties which will facilitate accurate analysis of superconducting coil structures.

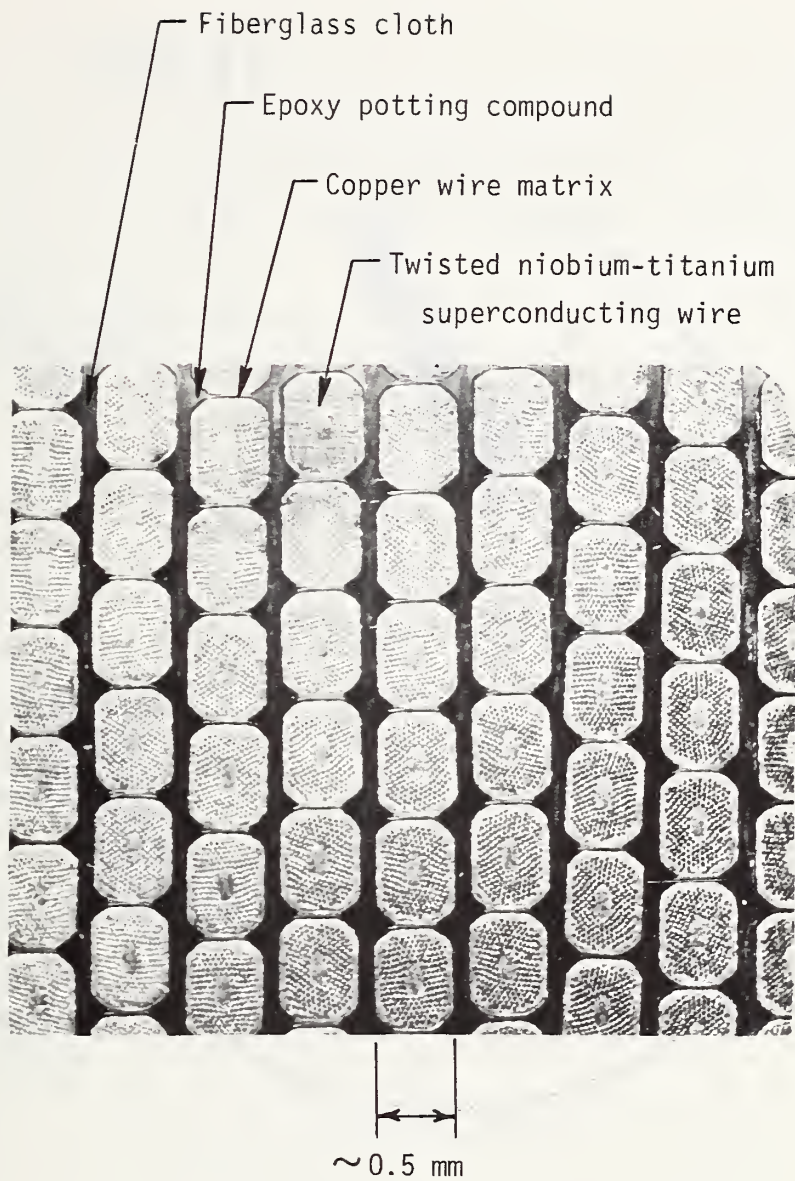


Figure 1. Cross section of the superconducting coil tested.

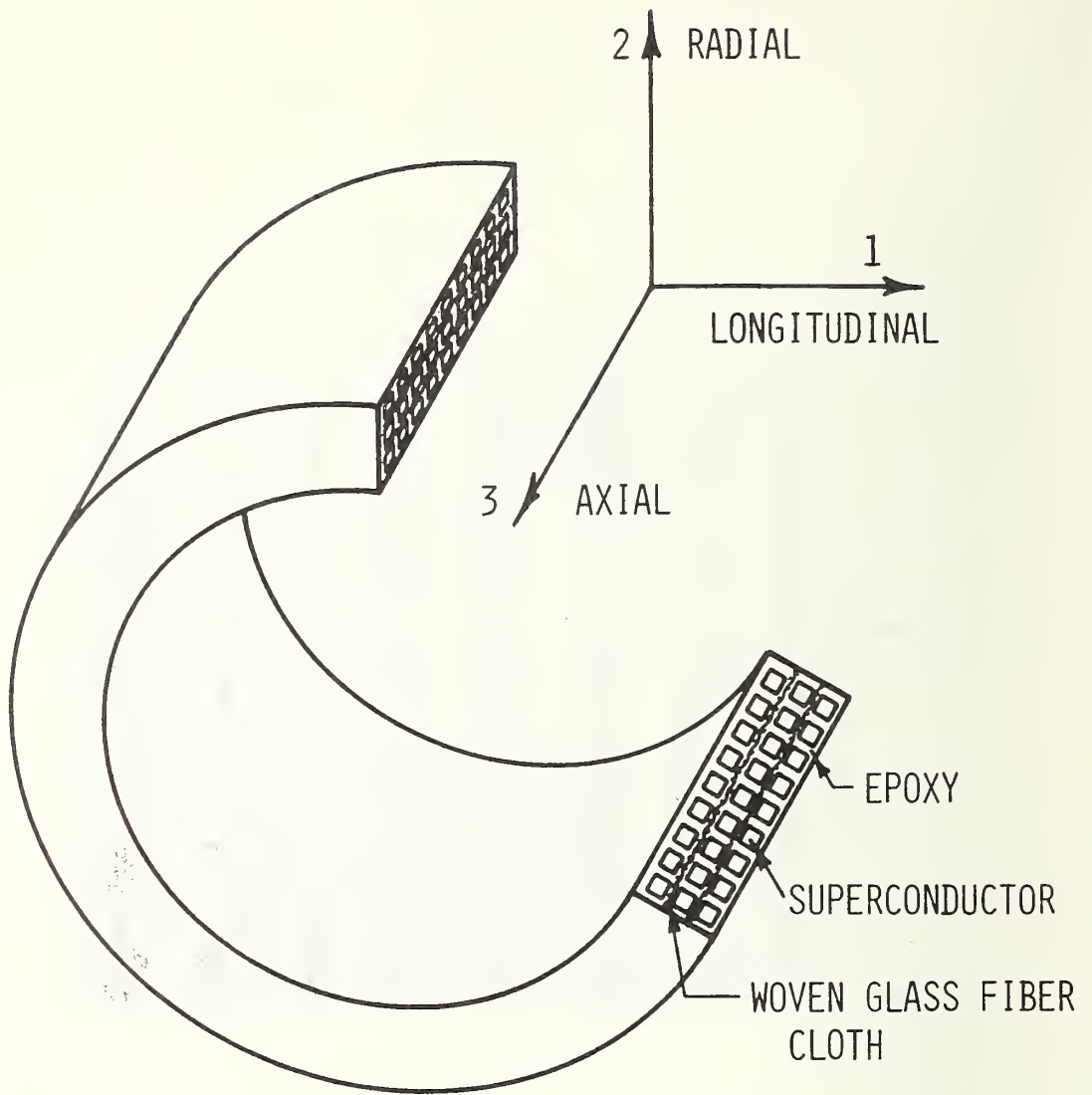


Figure 2. Schematic of solenoid coil showing construction and coordinate axes.

2. MACROSCOPIC MATERIAL PROPERTIES

To pursue the analyses discussed in the introduction, mechanical and thermal properties of the coil material must be measured. These properties include mechanical constitutive relationships, thermal expansions, conductivities, and diffusivities.

For a linear, elastic anisotropic solid the constitutive relationship is Hooke's law, which is given as [7]

$$\sigma_{ij} = c_{ijkl} \epsilon_{kl}, \quad i, j, k, l = 1, 2, 3 \quad (1)$$

where σ_{ij} and ϵ_{kl} are the stress and strain tensors. (Repeated indices are summed.) The constants c_{ijkl} can be measured in the laboratory and characterize the material. There are, in general, twenty-one independent constants.

The linear thermal expansion coefficients α_{ij} are defined by [8]

$$\epsilon_{ij} = \alpha_{ij} \Delta T \quad (2)$$

where ΔT is the temperature change. There are six independent thermal expansion constants. Similarly the thermal conductivity tensor k_{ij} is defined by [9]

$$-f_i = K_{ij} \frac{\partial T}{\partial x_j} \quad (3)$$

where f is the heat flux, T is the temperature, and x_j are Cartesian coordinates. There are six independent thermal conductivity constants.

The task of measuring the complete set of material properties for an anisotropic solid is difficult. However, there are several reasonable simplifications due to approximate material symmetries in the superconducting coil problem at hand.

2.1 Simplified Material Properties

The coordinate axes used to discuss the material properties of the coil material are illustrated in Figure 2. The anisotropic material properties

can be formulated more directly and simply if the coordinate axes are chosen to coincide with the natural or material axes. In Figure 2, the longitudinal or "1" axis coincides with the axis of the superconducting wire, which is assumed to have zero helix angle. The "2" and "3" axes lie along the radius and coil axis, respectively, and form an orthogonal set with the "1" axis.

The cylindrical symmetry of the coil reduces the number of independent elastic constants from 21 to 9, as for an orthotropic material [2,10]. Since this still represents a formidable and expensive series of laboratory tests, we choose for now to simplify the model still further by taking the reasonable approximation that the properties in the radial ("2") direction will be the same as in the axial ("3") direction. This model is termed transversely isotropic [2], and the number of constants required to characterize the material is now reduced to five. The accuracy of this approximation is discussed later, with reference to our experimental measurements.

It is convenient at this point to replace the tensor notation with the generally accepted contracted notation. Hooke's law is then written as

$$\sigma_i = C_{ij} \epsilon_j \quad i, j = 1, 2, \dots, 6 \quad (4)$$

where σ_i are the six stress components, and $\sigma_{ii} = \sigma_i$ for $i = 1$ to 3, $\sigma_{23} = \sigma_{32} = \sigma_4$, $\sigma_{13} = \sigma_{31} = \sigma_5$, and $\sigma_{12} = \sigma_{21} = \sigma_6$. C_{ij} is the stiffness matrix and ϵ_j are engineering strain components [10]. Alternatively the stress-strain relationships can also be represented in terms of the compliance matrix S_{ij} as

$$\epsilon_i = S_{ij} \sigma_j \quad (5)$$

The compliance matrix is the inverse of the stiffness matrix. It is convenient to introduce S_{ij} since its elements are more simply related to the familiar engineering constants: Young's modulus (E), Poisson's ratio (ν), and shear modulus (G). For a transversely isotropic, orthotropic material

$$\begin{aligned}
[S] = & \begin{array}{cccccc}
\frac{1}{E_{11}} & \frac{-\nu_{21}}{E_{22}} & \frac{-\nu_{21}}{E_{22}} & 0 & 0 & 0 \\
& \frac{1}{E_{22}} & \frac{-\nu_{23}}{E_{22}} & 0 & 0 & 0 \\
& & \frac{1}{E_{22}} & 0 & 0 & 0 \\
\text{(symmetrical)} & & & \frac{2(1+\nu_{23})}{E_{22}} & 0 & 0 \\
& & & & \frac{1}{G_{12}} & 0 \\
& & & & & \frac{1}{G_{12}}
\end{array} \quad (6)
\end{aligned}$$

where E_{11} and E_{22} are Young's moduli respectively in the 1 direction and in the isotropic 2-3 plane. ν_{ij} = Poisson's ratio = $(-1)\epsilon_j/\epsilon_i$, and G_{ij} is the shear modulus on the i plane in the j direction. Because the energy of a strained lattice is a scalar quantity, the matrix must be symmetrical [10], with the result

$$\frac{\nu_{21}}{E_{22}} = \frac{\nu_{12}}{E_{11}} \quad (7)$$

The same symmetry considerations, simplifications, and choice of axes lead to simplified thermal properties. The only non-zero components of the conductivity tensor K_{ij} , Equation (3), will be K_{11} , K_{22} , and K_{33} . Approximate transverse isotropy leads to $K_{22} \approx K_{33}$. Similarly all components of the thermal expansion tensor, Equation (2), are zero except α_{11} and $\alpha_{22} \approx \alpha_{33}$.

All of the material properties vary with temperature, which dictates measurements over a representative range of temperatures. Internal stresses due to construction and epoxy impregnation of the coil are developed at room temperature and above, while additional stresses due to thermal contraction and magnetic field develop at helium temperature. Experimental measurements must cover this range. This variation of material properties with temperature introduces additional complications into the stress analyses and heat transfer calculations.

3. MICROMECHANICAL ANALYSIS

In the field of structural composite materials considerable effort has been directed toward the prediction of the properties of a composite material given the properties and proportions of the constituent materials. These predictive procedures are usually derived from simplified micro-structure models using variational methods, theory of elasticity, or finite element analysis [10,11,12,13]. There exist a large number of rules for the prediction of elastic moduli and some rules for thermal properties. Such predictions are always approximations but can give results surprisingly close to measured macro-properties. It is instructive to predict the properties of the superconducting coil composite using micromechanics.

The photograph in Figure 1 shows the cross section of the coil in which four distinct phases can be identified: stranded superconductor, copper matrix, glass cloth, and epoxy. Most micromechanical predictive rules have been derived for only a two phase system, usually consisting of a fiber and a matrix material. Some modifications of the two phase rules could be made to accomodate four phases, but the equations would become much more complicated. At present an alternative is to introduce simplifying assumptions about the material that will reduce it to two phases. Since the glass cloth is only a small volume fraction it will be ignored in the calculations. The copper wire containing imbedded superconductor will be assumed to be a single material. The superconducting coil will thus be modeled by a two-phase system consisting of wires imbedded in an epoxy matrix.

Since some of the properties of the actual wire can be measured, the second assumption of a single material wire will not necessarily reduce the accuracy of the micromechanics analyses. The longitudinal Young's modulus of the wire has been measured at room temperature and is shown in Table 1. Measuring longitudinal thermal expansion and thermal conductivity of the wire presents no major experimental obstacles. However, transverse properties are difficult to measure to a useable degree of accuracy.

For estimation of the superconducting coil properties, nominal values of copper will be assumed if the wire property has not been measured. The epoxy matrix will also be given nominal values. All of the room-temperature constituent material properties used in subsequent micromechanics calculations are given in Table 1.

3.1 Volume-Fraction Determination

A cross section of an actual superconducting coil, Figure 1 was surveyed to estimate the volume fraction of wire in the coil. The schematic of the coil cross section is shown in Figure 3, which presents average values of wire dimensions and wire spacings in the axial and radial directions.

Note that the spacing of the wires differs considerably in the 2 and 3 directions contrary to the earlier assumption of isotropy in the 2-3 plane. Since properties normal to the wire are very sensitive to the wire spacing, an adjusted set of volume fractions were computed separately for the 2 and the 3 directions. For example, since small spacings between wires are normal to the 2 direction, for some theoretical calculations the volume fraction should be computed by assuming that all spacings are small. Similarly for the 3 direction, an effective volume fraction is computed by assuming that all of the wire spacings have the larger value. The fiberglass is ignored because of its very small volume fraction.

Many of the theoretical solutions are based on an analytical model consisting of a square array of circular filaments imbedded in a matrix [14,15]. But, the superconducting coil wires tend toward rectangular shape. Because of this discrepancy another effective volume fraction was calculated. For this calculation it was assumed that the coil was made up of circular wires with diameters equal to the appropriate dimensions of the actual wires and with spacings identical to those of the actual wires. These equivalent volume fractions were computed for the 2 and the 3 directions and are shown in Table 2. These values necessarily fall somewhere below and above the actual volume fraction, respectively. The tabulated values include corrections for rounding of the corners of the nominally-square wire.

Table 1. Room temperature constituent material properties
for micromechanics calculations.

	Superconducting Wire	Copper ^(b)	Epoxy ^(b)
E 10^4 MN/m ² (10^6 psi)	7.85-8.20 ^(a) (11.4-11.9)	11.7 (17)	0.34 (0.49)
ν	0.33 ^(c)	0.345	0.29
G 10^4 MN/m ² (10^6 psi)	3.00 ^(c) (4.36)	6.3 (9.1)	0.19 (0.28)
α K ⁻¹ (°F ⁻¹)	----	17.6 (9.8)	45.0 (25.0)
k W/mK (Btu/hr ft F)	----	387 (224)	0.35 (0.2)

(a) Longitudinal modulus, measured at NBS, 8.03×10^4 MN/m² (11.65×10^6 psi) used for calculations. In review, we note that our stress-strain data is significantly non-linear, and that this stated modulus is valid for stresses of about 4 to 7 x 10^4 MN/m² (5 to 10 ksi). The measured modulus is lower at lower stress levels. We will investigate this non-linearity quite carefully in future work.

(b) Nominal values.

(c) Assumed values.

Table 2. Equivalent volume fractions for transverse directions.

		Volume Fraction of Wire, Average Values
Actual cross section of coil	(measured)	0.73
Assume uniform spacing of 0.03175 mm (0.00125 in.) for properties along 3 axis		
Actual wire	(calculated)	0.803
Equivalently spaced square array of circles	(calculated)	0.72
Assume uniform spacing of 0.1067 mm (0.0042 in.) for properties along 2 axis		
Actual wire	(calculated)	0.652
Equivalently spaced square array of circles	(calculated)	0.55

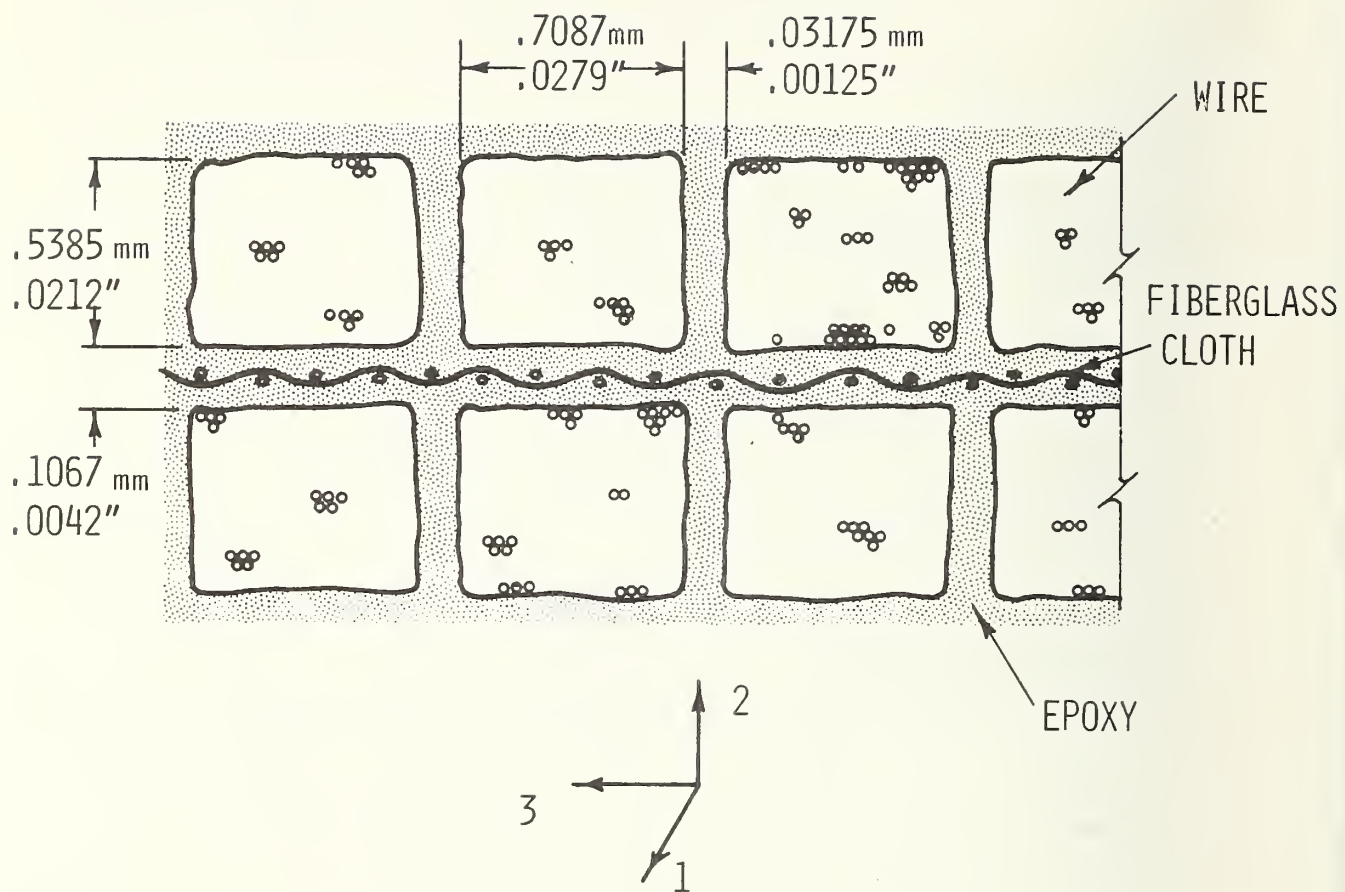


Figure 3. Average spacing of coil composite wires.

3.2 Predictive Laws

An elementary set of predictive laws can be derived from the parallel and series models shown in Figure 4. Young's modulus (E) for the parallel model is

$$E_c = V_f E_f + V_m E_m \quad (8)$$

where V is the volume fraction and the subscripts f, m and c denote properties associated with the fiber, matrix, and composite respectively. For the superconducting coil the wires are considered as fibers and the epoxy potting compound as the matrix.

Equation (8) is commonly referred to as "the law of mixtures". It can be shown using the principle of minimum potential energy that the modulus given by Equation (8) is an upper bound for the composite modulus [10], but gives a reasonably accurate estimate of longitudinal modulus for structural composites [16].

If shear stresses are ignored the series model yields the equation

$$E_c = \frac{E_f E_m}{E_f V_m + E_m V_f} \quad (9)$$

for the composite modulus. By applying the principle of minimum complementary energy it may be shown that Equation (9) is a lower bound on E_c .

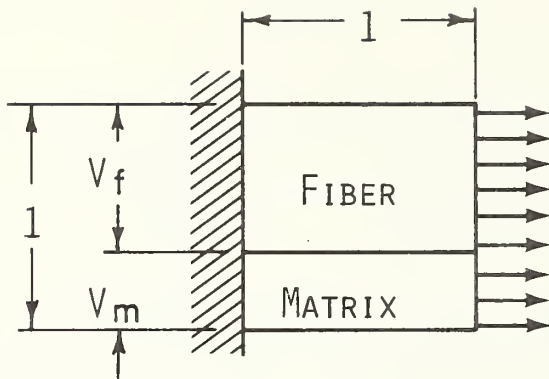
Equations for thermal expansion of the parallel and series models can similarly be obtained if shear stress and bending are ignored. The parallel model yields

$$\alpha_c = \frac{\alpha_f V_f E_f + \alpha_m V_m E_m}{E_c} \quad (10)$$

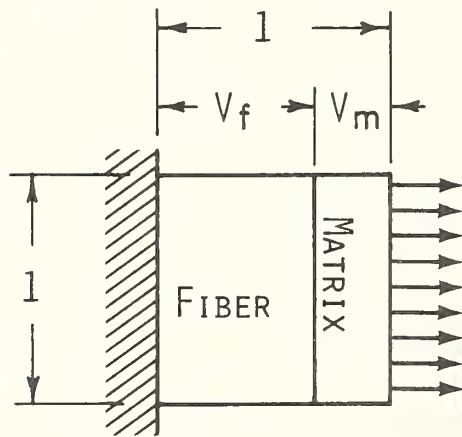
and the series model yields

$$\alpha_c = V_f \alpha_f + V_m \alpha_m \quad (11)$$

where α denotes the linear coefficient of thermal expansion [17].



PARALLEL MODEL



SERIES MODEL

Figure 4. Two simple micromechanical models of a composite material.

The composite thermal conductivity for the parallel model will be

$$K_c = V_f K_f + V_m K_m \quad (12)$$

where K denotes thermal conductivity. The elements of the model are assumed to be separated by an infinitesimal adiabatic plane [18]. The series model yields

$$K_c = \frac{K_f K_m}{K_m V_f + K_f V_m} \quad (13)$$

The contact resistance is assumed to be zero between the elements, and the temperature distribution is assumed to be one dimensional. For reference the micromechanical equations for the series and parallel models are shown in Table 3.

Poisson's ratio (ν) can be derived from the parallel model and is given as [19]

$$\nu_{12} = \nu_{13} = V_f \nu_f + V_m \nu_m \quad (14)$$

The first subscript in this notation always denotes the direction of applied stress, while the second subscript denotes the direction of the Poisson contraction. Equation (7) is used to obtain ν_{21} from ν_{12} or vice versa.

Using variational methods, Rosen et al., [20,21] derived an expression for ν_{13} for a random array of fibers. The equation is

$$\nu_{13} = \frac{V_f E_f L_1 + V_m E_m L_2 \nu_m}{V_f E_f L_3 + V_m E_m L_2} \quad (15)$$

where

$$L_1 = 2\nu_f(1 - \nu_m^2)V_f + V_m(1 + \nu_m)\nu_m$$

$$L_2 = V_f(1 - \nu_f - 2\nu_f^2)$$

and

$$L_3 = 2(1 - \nu_m^2)V_f + (1 + \nu_m)V_m.$$

Table 3. Elementary micromechanics equations for predicting composite properties

	Parallel Model	Series Model
Composite Young's Modulus, E_c	$V_f E_f + V_m E_m$ <p>(upper bound)</p>	$\frac{E_f E_m}{E_f V_m + E_m V_f}$ <p>(lower bound)</p>
Composite Thermal Expansion α_c	$\frac{\alpha_f V_f E_f + \alpha_m V_m E_m}{E_c}$	$V_f \alpha_f + V_m \alpha_m$
Composite Thermal Conductivity k_c	$V_f k_f + V_m k_m$	$\frac{k_f k_m}{k_m V_f + k_f V_m}$

The remaining Poisson's ratio ν_{23} is obtained using the equation [11]

$$\nu_{23} = \nu_f V_f + \nu_m V_m \left\{ \frac{1 + \nu_m - \nu_{13} (E_m/E_{11})}{1 - \nu_m^2 + \nu_m \nu_{13} (E_m/E_{11})} \right\} \dots \quad (16)$$

The shear modulus in the plane of isotropy, 2-3, can be computed using the relationship among elastic constants of isotropic materials. For example, if E_{33} and ν_{23} are known, then G_{23} is given by the familiar relationship

$$G_{23} = \frac{E_{33}}{2(1 + \nu_{23})} \quad (17)$$

The shear modulus in the 1-3 plane is an independent material property and must be measured or calculated from a micromechanics.

Assuming a simple model containing rectangular fibers, Ekvall [19] derived

$$G_{13} = \frac{G_f G_m}{V_m G_f + V_f G_m} \quad (18)$$

for a lamina one filament thick.

Using variational methods Rosen, et al. [20,21] obtained upper and lower bounds for the shear modulus. These are given as

$$G_{13} \text{ (upper bound)} = G_m (m_G V_1 + V_2) \quad (19)$$

and

$$G_{13} \text{ (lower bound)} = \frac{G_m}{(V_1/m_G + V_2)} \quad (20)$$

where

$$m_G = \frac{\eta(1 + \beta^2) + 1 - \beta^2}{\eta(1 - \beta^2) + 1 - \beta^2}$$

and $\eta = G_f/G_m$, $\beta = V_f/V_1$, $V_1 = \pi/2\sqrt{3} = 1 - V_2$. For a random array of fibers the bounds coincide and the modulus is given as

$$G_{13} = G_m \frac{\eta(1 + V_f) + V_m}{\eta V_m + 1 + V_f} . \quad (21)$$

Another expression for G_{13} derived by Foye [22] has been found to be in good agreement with elasticity solutions for regularly spaced arrays. It is

$$G_{13} = \frac{G_m}{2} \frac{4 - \pi + \pi N}{4} + \frac{4N}{(4-\pi)N + \pi} \quad (22)$$

where

$$N = \frac{G_f(\pi + 4V_f) + G_m(\pi - 4V_f)}{G_f(\pi - 4V_f) + G_m(\pi + 4V_f)} .$$

The equations presented in these sections on micromechanics are representative of the predictive equations available to the experimentalist and analyst. Other valuable tools for modulus prediction are found in a number of elasticity and finite element solutions for the transverse properties of regular arrays of fibers [11,14,15]. Comparison of experimental results with those predicted by the above relationships will be made in a later section.

4. SPECIMENS

All specimen fabrication was performed by the sponsor using superconducting wires, epoxies, bonding techniques, etc. selected by them to meet their program needs. The information in this section on sample preparation was obtained from the sponsor.

To measure the properties in the 1 direction, specimens were prepared using straight wires, Figure 5a. In order to make these specimens representative of the actual material in the coil, efforts were made to reproduce the volume fractions of the components as well as the curing procedure.

To measure properties in the 2 and 3 directions, blocks were sectioned from an actual coil. These blocks were then fabricated into specimens with thin epoxy bond lines. A schematic of this specimen is shown in Figure 5b along with the coordinate system relating the specimen orientation to the coil, Figure 2.

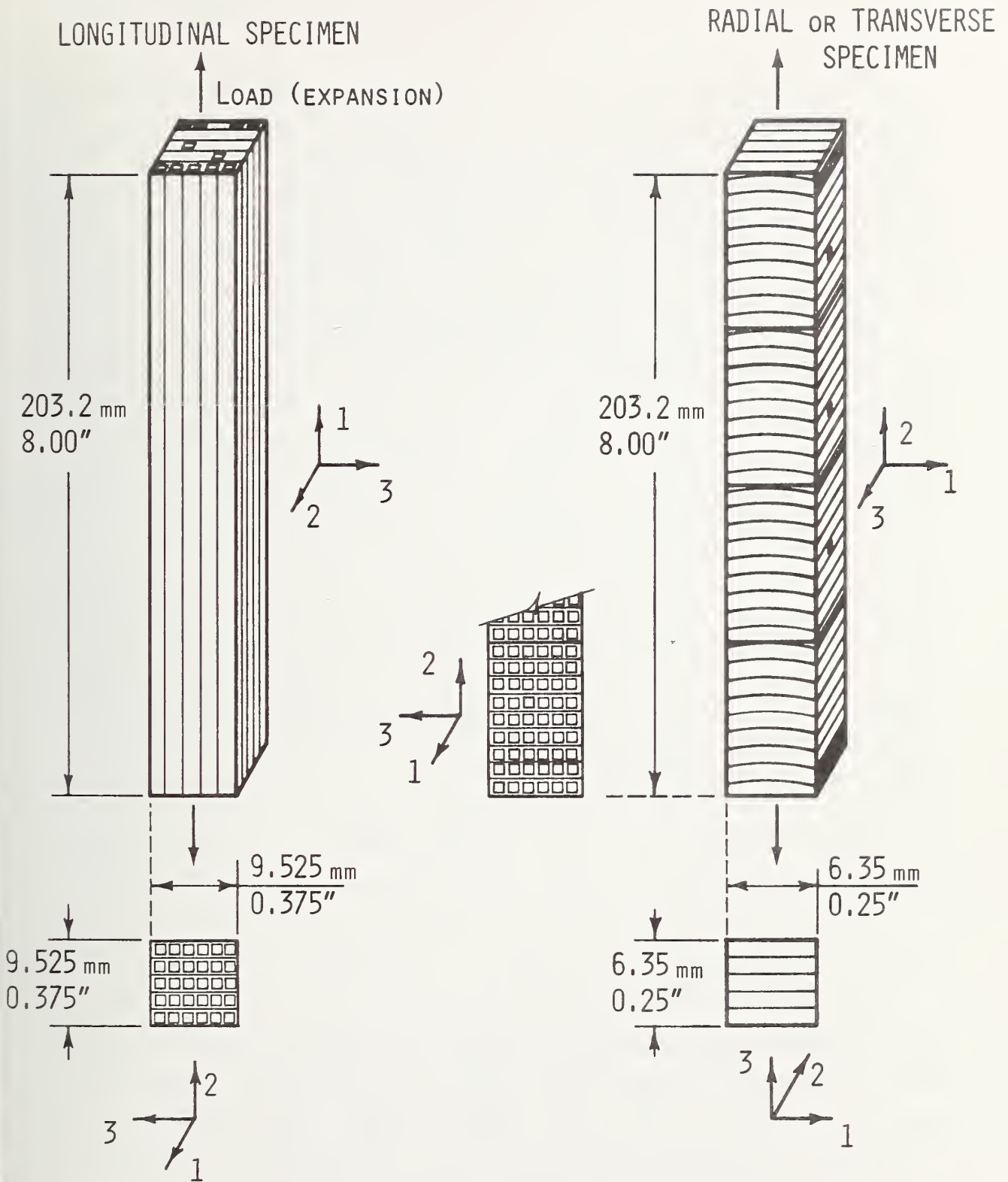


Figure 5. Schematic of specimen structures and orientations
 (a) Longitudinal specimen (b) Radial or transverse specimen

The superconducting wire used to wind the test coil and to produce the longitudinal specimens was multifilament niobium-titanium embedded in a copper matrix. The copper-to-superconductor volume ratio is 1.8 to 1. There are 180 superconducting strands having a twist pitch of 2 per inch. The conductor is rectangular in cross-section measuring .56 mm (.022 in.) by .72 mm (.0285 in.) including .020 mm (.0008 in.) electrical insulation.

The test coil was a simple solenoid containing 40 layers of wire. The coil has an inside diameter of 19.38 cm (7.632 in.), an outside diameter of 24.47 cm (9.632 in.) and a length of 10 cm (4 in.). The wire was wound on a stainless steel coil form (mandrel). Before the wire is applied to the mandrel it is cleansed of any residual oil and contaminants, and pretensioned. A wire guide and "finger" mechanism were used to place the wire in its exact final position on the mandrel. This mechanism also provided approximately 2 lbs (9N) of side force to establish excellent wire packing horizontally. The wire was cleaned after leaving the supply reel by drawing it through a solvent jet and several felt wiping pads. The pretension was developed by applying reverse torque to the supply reel. The following pretension was used in winding the test coil.

<u>layer</u>	<u>tension (lbs.)</u>	(N)
1 thru 10	17.6	(78.3)
11 20	13.2	(58.7)
21 30	8.8	(39.1)
31 40	4.4	(19.6)

The wire used to fabricate the longitudinal samples was pretensioned to 8.8 lbs (39N). Before the first turn of wire was wound, one complete layer of fiberglass cloth, .1 mm (.004 in.) thick, 3 oz. per sq. yd. ($\sim 100 \text{ gm/m}^2$) was applied to the coil form. The fiberglass had approximately .6 cm (1/4 in.) overlap at the ends and .3 cm (1/16 in.) turn up, approximately two wire thicknesses, at the side flanges. The overlap and turn up are necessary to provide reinforcement for the epoxy in these critical areas. A layer of wire is then wound over the dry

fiberglass. Just after the wire moves up to the next layer another layer of dry fiberglass cloth is installed in the same manner as the first layer. The second layer of wire then proceeds as the first. The winding procedure continues layer on layer until the coil is complete.

Mechanical measurements of the superconducting test coil were made after winding, showing it to be very uniform. The maximum radial runout over the entire surface of the coil was $\pm .15$ mm (.006 in.).

After the superconducting coil is completely wound it is placed in a potting mold slightly larger than the coil outside diameter. The coil is then placed in a vacuum chamber and evacuated to approximately 10^{-2} torr (1.33 N/m^2). This pressure is maintained for 8 hours at which time the chamber heaters are turned on and the coil is raised to 150°F (65°C). After the coil, fiberglass, and chamber have fully degassed, they are ready to receive the epoxy resin.

The epoxy used in the superconducting coil is Ciba 6005*. The epoxy is preheated to 150°F (65°C) then degassed to a pressure of 5×10^{-2} torr (6.7 N/m^2). This process takes approximately 15 minutes. After degassing is complete the epoxy is piped into the potting mold until the entire coil is completely covered. Then the chamber containing the coil is pressurized to 100 psig ($.69 \text{ MN/m}^2$). This pressure is held for 8 hours at 150°F (65°C), until the epoxy system is entirely cured. The temperature is then slowly decreased to 77°F (25°C) and the chamber is vented to atmospheric pressure. The coil is then taken out of the chamber, and the potting mold and all excess epoxy removed. The coil is now complete. The same process was used for the longitudinal specimens.

*The use in this paper of trade names of specific products is essential to a proper understanding of the work presented. Their use in no way implies any approval, endorsement, or recommendation by NBS.

5. THERMAL EXPANSION MEASUREMENT

5.1 Procedure

The low temperature thermal expansion of the specimens was measured using a quartz tube dilatometer from room temperature to 4 K utilizing the apparatus of Clark [23]. The specimen, approximately 20 cm (8 in.) long, is slowly cooled by helium exchange gas after the apparatus is immersed in a cryostat containing liquid nitrogen. When the specimen has reached 77 K, the cryostat is purged of liquid nitrogen and filled with liquid helium. Cooling at a rate of 2-5 K/min was chosen as the best compromise between speed of measurement and minimal temperature gradients in the specimens. Using this cooling rate, the test took 3-4 hrs., which includes 1 hr for purging of liquid nitrogen and filling with liquid helium. The differential contraction is transmitted to a mechanical dial gauge at room temperature by concentric quartz tubes. A schematic of the apparatus is shown in Figure 6. The temperature of the specimen is determined by two chromel-constantan thermocouples attached directly to opposite sides of the specimen, one about 5 cm (2 in.) down from the top of the specimen and the other about 5 cm (2 in.) up from the bottom. This procedure gave rise to data pairs that could be averaged to effectively eliminate thermal gradients in the specimen [23]. The thermocouples were calibrated following the procedure of Sparks and Powell [24].

Five specimens were tested: two radial, and two longitudinal coil sections and one longitudinal epoxy-fiberglass. The specimens were fabricated to the dimensions $20 \pm .5$ cm (8 in. \pm 1/4 in.) long and approximately 1 cm (3/8 in.) square, with the exception of the radial specimens that were made from a stack of 2.5 x .63 x .63 cm (1 in. x 1/4 in. x 1/4 in.) radial segments epoxied end to end. The specimens are shown in Figure 7a.

This type of thermal expansion measurement is relative and must be compared to a similar specimen of a known material. The calibration of the apparatus was accomplished by repeated measurements of a specimen machined from NBS Standard Reference Material 736, an OFHC copper reference standard

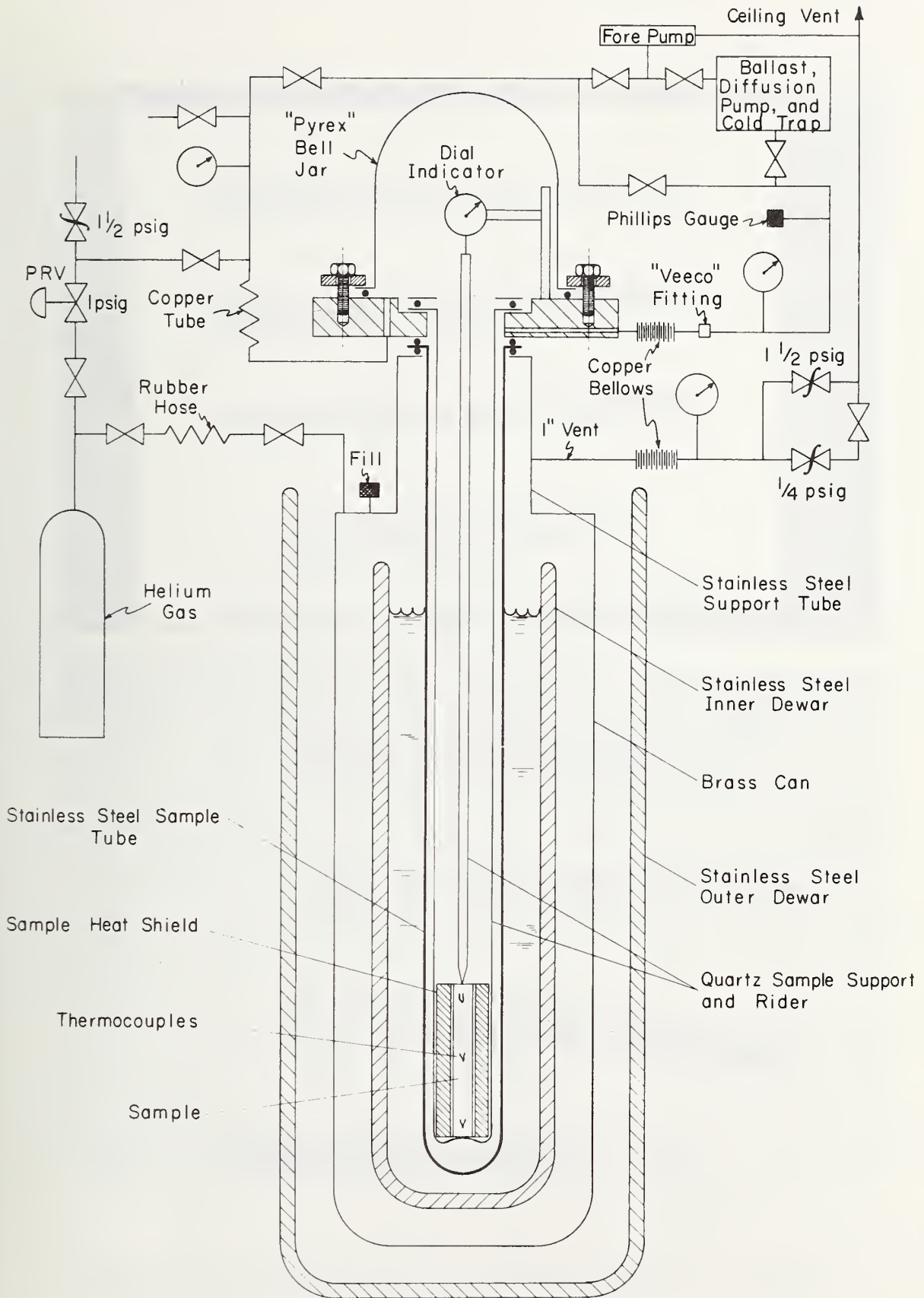


Figure 6. Schematic of thermal expansion apparatus.

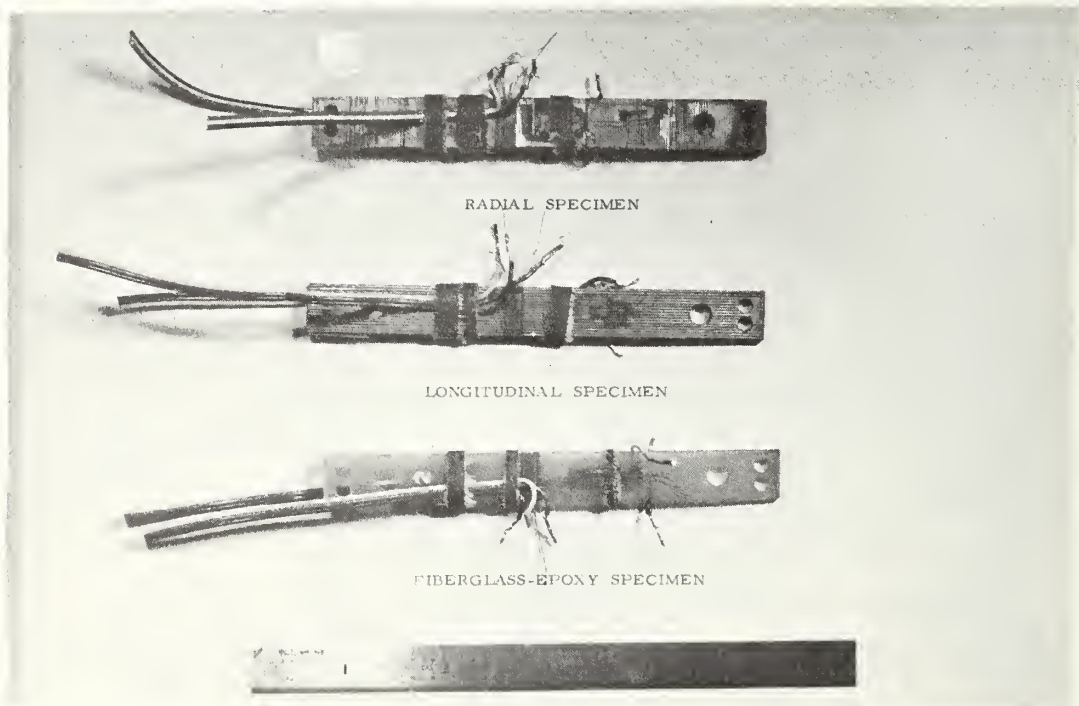
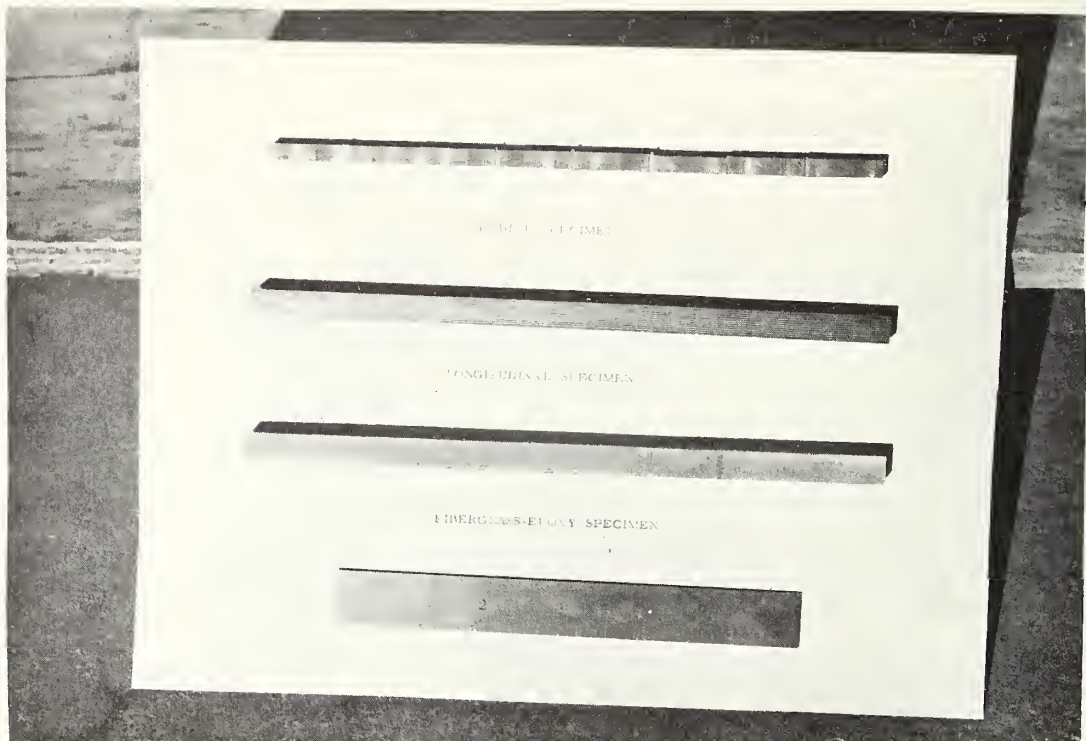


Figure 7. Thermal expansion (a) and tensile (b) specimens.

available from the Office of Standard Reference Materials, National Bureau of Standards, Washington, D.C. The specimen was stress relieved at 1112°F (600°C) for 1 hour before testing. The reproducibility of the calibration was better than 0.3%. The high degree of reproducibility was maintained throughout the test program. The difference between an average of this calibration data and the primary standard reference data accounts for residual differential contractions in the quartz tubes, and was used as a correction to all other specimen measurements. The correction (Table 4) was less than 5% throughout the temperature range.

5.2 Data

A computer curve-fitting program was developed to fit the experimental data and to reduce the data to standard tabular form. Several polynomials in temperature were tried and simple power series limited to T^5 were usually best. The expansion coefficient ($\alpha \text{ K}^{-1}$) was obtained by taking the derivative of each equation. The final tabular values were determined by visual inspection of each of the curve fits; the fit to the thermal contraction being selected if the curve visually fit the data points and the corresponding derivative was "regular" (i.e., approached $T = 0$ as T^3 and approached a constant at the higher temperatures).

The data are compiled in a standard tabular form in Table 4 showing both the thermal expansion referred to room temperature, $(L_{293} - L_T)/L_{293}$, and the thermal expansion coefficient, $\alpha = (1/L_{293})(dL/dT)$. The best approximation of a single equation for each specimen is presented as curves for both the thermal contraction and the thermal expansion coefficient in Figures 8 and 9.

The variation between selected values for the averaged curve fits was at most $\pm 1.0 \times 10^{-5}$ or $\pm 1\%$, whichever is greater, for the thermal contraction values; for the thermal expansion coefficient values the variation was at most $\pm 0.1 \times 10^{-6} \text{ K}^{-1}$ or $\pm 2\%$, whichever is greater. This accuracy is probably greater than the differences that might be expected due to variability among composite specimens made in different ways. Nevertheless, the values measured should be representative of this type of composite within $\pm 5\%$ for an equivalent volume fraction.

Table 4. Linear Thermal Contraction and Coefficient of Linear Thermal Expansion for Superconducting Coil Materials

T (K)	Radial # 1		Radial # 2		Longitudinal # 1		Longitudinal # 2		Fiberglass Epoxy		Calibration Correction $10^5 \frac{L_{293} - L_T}{L_{293}}$
	$10^5 \frac{L_{293} - L_T}{L_{293}}$	$10^6 \frac{dL}{dT}$ (K ⁻¹)	$10^5 \frac{L_{293} - L_T}{L_{293}}$	$10^6 \frac{dL}{dT}$ (K ⁻¹)	$10^5 \frac{L_{293} - L_T}{L_{293}}$	$10^6 \frac{dL}{dT}$ (K ⁻¹)	$10^5 \frac{L_{293} - L_T}{L_{293}}$	$10^6 \frac{dL}{dT}$ (K ⁻¹)	$10^5 \frac{L_{293} - L_T}{L_{293}}$	$10^6 \frac{dL}{dT}$	
0	473a	0	474a	0	274a	0	278a	0	262a	0	-12.5
10	473	0.4a	474	0.3a	274	0.07a	278	0.04a	262	1.5	-12.4
20	472	2.1	473	1.7	274	0.5	278	0.6	260	2.6	-12.3
30	467	4.4	469	3.7	273	1.4	277	1.4	256	3.7	-12.2
40	463	6.5	465	5.9	271	2.5	275	2.6	252	4.5	-11.8
50	456	8.4	458	7.9	268	3.7	272	3.8	248	5.3	-11.0
60	446	10.1	449	9.8	262	5.1	268	4.9	242	6.0	-10.0
70	435	11.6	438	11.5	257	6.3	262	6.0	235	6.7	-8.9
80	423	13.0	426	12.9	250	7.4	256	7.1	229	7.4	-8.0
90	409	14.2	412	14.2	243	8.4	248	8.0	221	8.0	-7.0
100	395	15.2	397	15.3	234	9.2	240	8.9	213	8.5	-6.4
120	362	17.0	365	17.3	214	10.7	220	10.5	195	9.5	-5.5
140	327	18.4	329	18.7	191	11.6	198	11.8	175	10.2	-4.9
160	289	19.5	290	19.8	172	12.3	176	12.7	154	10.9	-4.8
180	249	20.5	249	20.6	146	12.6	152	13.3	132	11.3	-4.8
200	206	21.2	207	21.3	121	12.8a	125	13.5a	109	11.6	-4.8
220	165	21.8	164	21.8	94.8	12.8a	97.7	13.5a	85.3	11.7	-4.6
240	120	22.3	120	22.2	69.2	12.8a	70.8	13.5a	61.9	11.7	-3.9
260	75.5	22.7	75.9	22.6	43.5	12.8a	43.9	13.5a	38.5	11.7	-2.8
273	48.2	22.9	48.6	22.8	26.8	12.8a	26.4	13.5a	24.4	11.7	-1.8
280	30.2	23.0a	30.6	22.9a	17.8	12.8a	17.0	13.5a	15.2	11.7	-1.2
293	0.	23.2a	0.0	23.1a	0.0	12.8a	0.0	13.5a	0.0	11.8	0.0
300	-15.9	23.3a	-16.1	23.2a	-7.8	12.8a	-9.9	13.5a	-8.2	11.8	0.7

a Extrapolated.

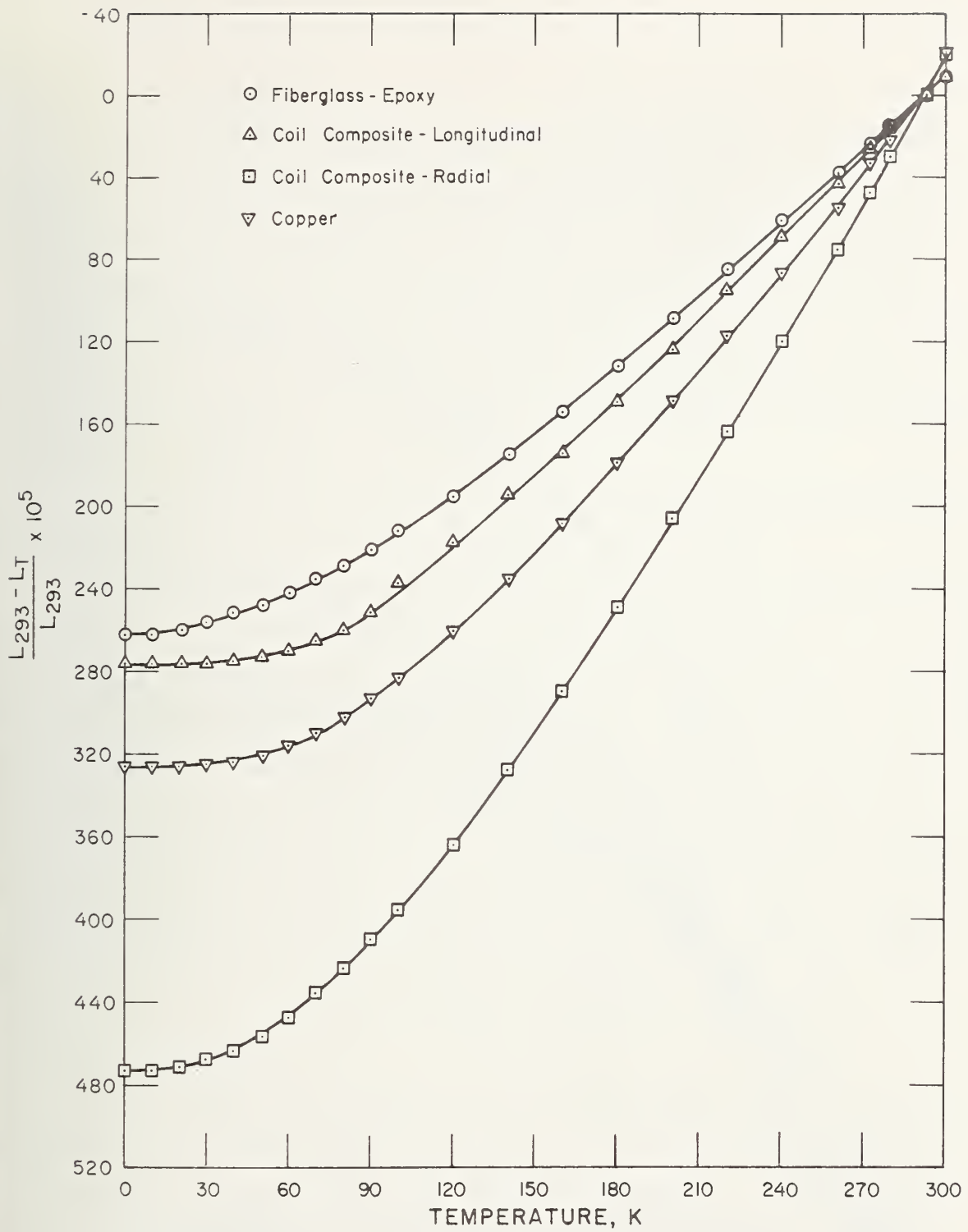


Figure 8. Thermal contraction of superconducting coil materials.

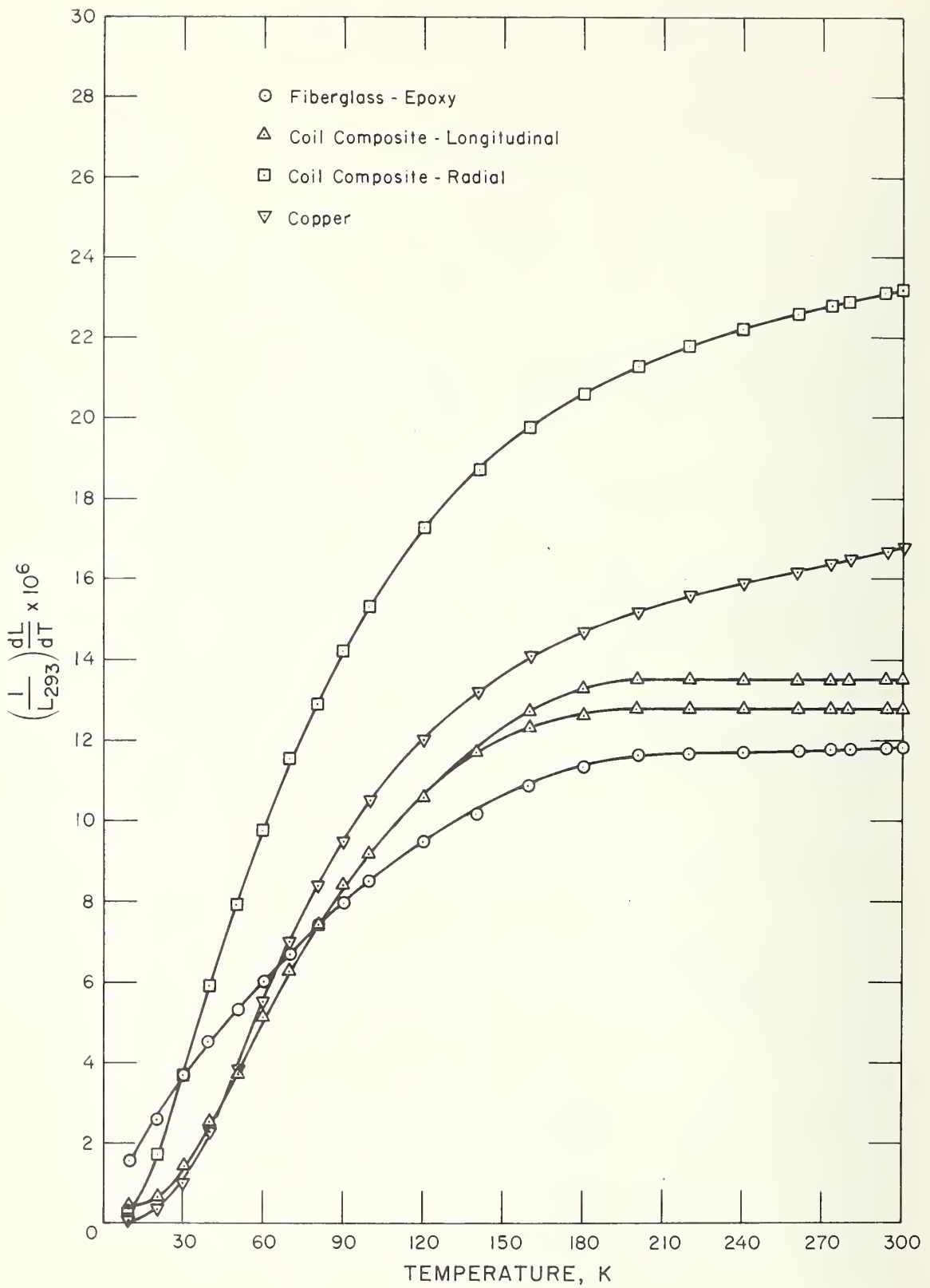


Figure 9. Thermal expansion coefficient of superconducting coil materials.

5.3 Discussion

The radial specimens showed nearly twice the thermal contraction of both the longitudinal and the fiberglass specimens. This is consistent with the known large thermal contraction of pure epoxy [26], and the fact this orientation is more accurately represented by the series model, Equation (11), than the parallel model, Equation (10). The approximate equality of the contractions of the fiberglass and the longitudinal coil specimens shows that fiberglass, like the metallic conductors, inhibits the thermal contraction of the epoxy.

The relatively large expansivity of the fiberglass specimen below 70 K is apparently real, but is not understood at this time.

The important feature of this result is that the coil structure tends to contract significantly more in the radial direction than in the longitudinal direction. This means that, at 4 K prior to energizing the coil, the superconducting wire will experience stresses due to additive effects of winding tension during fabrication and thermal contraction during cooldown. Further, the coil will tend to contract more than the fiberglass-epoxy overwrap. Both of these may diminish the allowable magnetic field pressure which the coil can tolerate before yielding. These effects need careful investigation, and analytical studies in this direction are proceeding.

6. YOUNG'S MODULI AND POISSON'S RATIOS

6.1 Procedure

Young's moduli and Poisson's ratios were measured for three specimen orientations at room temperatures as well as at the normal boiling points of nitrogen, 77 K (-320°F), and helium, 4 K (-425°F). Tensile specimens were instrumented with strain gages, as shown in Figure 10. Gages were placed longitudinally (along the axis of pull) in order to measure Young's modulus, i.e., strain in the longitudinal direction, as well as transversely (90° to the direction of pull) to measure strain due to the Poisson effect. Corresponding gages on opposite faces were connected in series to eliminate any spurious output due to bending.

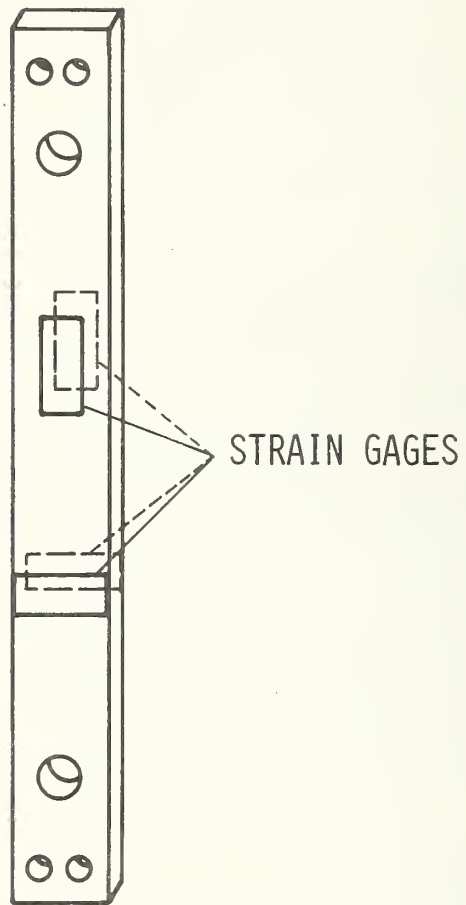


Figure 10. Strain gage location on tensile specimens.

Specimens were tested on a universal testing machine (Figure 11). The lower specimen grips were attached to the support frame, which in turn was secured to the movable cross-beam of the test machine. The upper grips were connected via a .63 cm (1/4 in.) titanium rod to the load cell, mounted at the top of the testing machine.

For tests in nitrogen (liquid), a slit-silvered dewar was placed around the test frame. For runs at helium temperatures, an additional outer "shield" dewar was mounted around the inner dewar and filled with LN₂. After purging the fill tubes and inner dewar with helium gas, liquid helium was transferred until the liquid level rose above the upper specimen grips. One filling lasted for 1-1/2 hours, sufficient for several series of runs.

The strain gages were attached to a Wheatstone bridge balance, and the circuit was initially balanced. During loading and unloading, the resulting imbalance was then amplified and read as an apparent strain on an X-Y recorder. The output of the load cell was connected to the remaining axis (Figure 12). Typical resulting curves are shown in Figure 13.

Between 5 and 10 runs were made for each set of gages at each temperature, whereafter the complementary gages were connected. The system bridge was rebalanced, the load-unload test sequences were repeated, and the output was recorded on the same piece of graph paper for easy comparison. Since there was a small loading and unloading hysteresis, only that portion of the test curve above and below this effect was used. From each set of test curves, two were designated "representative" and values from them were averaged.

Longitudinal specimens were loaded to about 83 MN/m² to 110 MN/m² (12000 - 16000 psi). At loads much above this, the specimens would break at the grip holes. Therefore, as an added precaution, the grips were epoxied to the specimens, and an epoxy fillet was added along the grip-specimen boundaries. Similarly, in order to keep within the elastic ranges, the fiberglass-epoxy specimen was loaded to only 55 MN/m² (8000 psi).

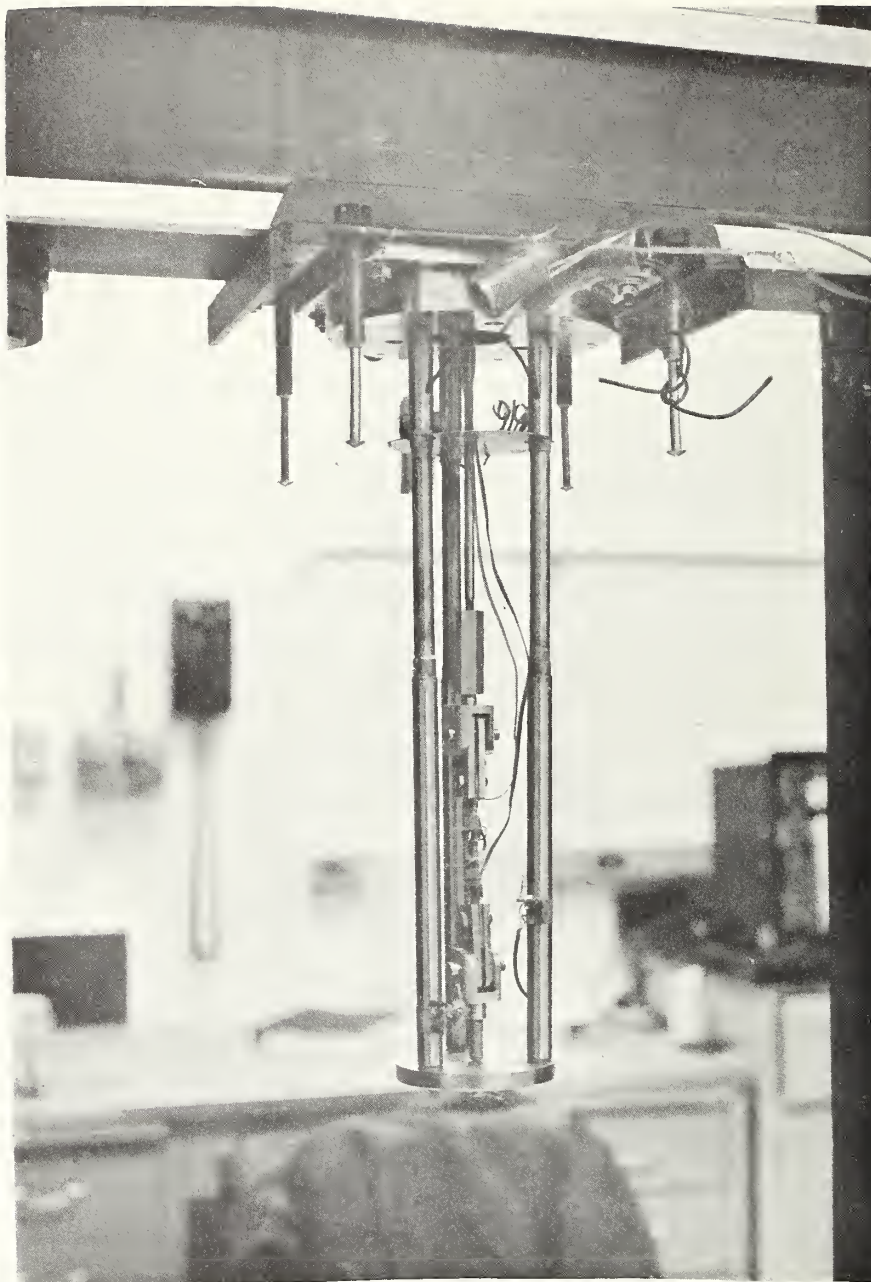


Figure 11. Tensile test apparatus.

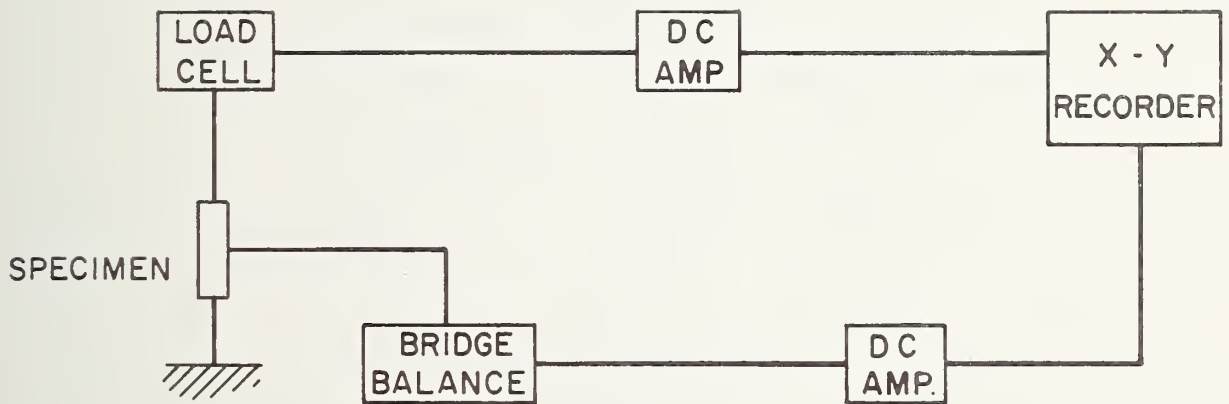


Figure 12. Schematic of gage circuit.



Figure 13. Typical apparent stress strain curve.

Since the radial tensile specimens were fabricated from sections of an actual coil which were epoxied together, loads were kept to about 5.5 MN/m^2 (800 psi). The epoxy bond at the butt-joints failed at loads about 7 MN/m^2 (1000 psi). Load was converted to stress by the relationship

$$\sigma_a = L/A \quad (23)$$

where

σ_a = apparent stress;

L = load, i.e., measured output of load cell;

A = cross sectional area of the specimen, measured at the gage.

True strain was calculated from apparent strain, compensating for transverse gage effects by the following formulae:

$$\epsilon_l = \frac{(\epsilon_{l_a} - k\epsilon_{t_a})(1 - \mu_0 k)}{(1 - k^2)} \quad (24)$$

$$\epsilon_t = \frac{(\epsilon_{t_a} - k\epsilon_{l_a})(1 - \mu_0 k)}{(1 - k^2)} \quad (25)$$

where

ϵ_l = true longitudinal strain

ϵ_t = true transverse strain

ϵ_{l_a} = apparent longitudinal strain

ϵ_{t_a} = apparent transverse strain

k = transverse correction factor, = -0.034

μ_0 = Poisson's ratio of the material upon which strain gage was calibrated (1018 Steel), = 0.285.

These corrections were negligible for the longitudinal gages (< 1%), but proved to be considerable (~ 20%) for the transverse gages.

Since gage factors vary as a function of temperature, corrections had to be made to the strain gage output whenever tests were done at temperatures other than room temperature. These corrections were taken from curves supplied by the manufacturer of the strain gages, extrapolated to include the data taken at helium temperatures.

6.2 Data

From the true strains, Young's modulus and Poisson's ratio were calculated from

$$E = \frac{L/A}{\epsilon} \quad (26)$$

and

$$\nu = - \frac{\epsilon_t}{\epsilon_l} \quad (27)$$

The data are plotted in Figures 14 and 15 and listed in Table 5.

Instrument errors are nominally set at $\pm 0.5\%$, this being the uncertainty quoted for the electrical components. The gage factors are $\pm 1\%$, at room temperature, but may be higher at low temperature which leads to an estimated error for the longitudinal and fiberglass-epoxy specimens of about 2 or 3%.

Since the radial specimens were so fragile, loads were kept to 5.5 MN/m^2 (800 psi) or less. The resulting strains were quite small (on the order of 10^{-4} for the Poisson gage output), and the noise level resulted in resolution errors several times higher than the above uncertainty. These instrumental errors are probably small compared to variability which could reasonably be expected in the composite sample fabrication.

6.3 Discussion

Young's modulus of every specimen decreased slightly with increasing temperature, as shown in Figure 14. Poisson's ratio also appears to decrease with increasing temperature, Figure 15, but the curvature is of opposite sign. The 4 K (-452°F) data point for radial specimen # 1 may be in error. The large variations in Poisson's ratio between the two radial specimens may be due to markedly different compositions, different curvatures in the respective constituent wires, or perhaps to local debonding near the strain gage. This is being investigated further.

The general behavior is similar to the thermal expansion in that the longitudinal moduli are similar to the superconducting copper wire and the transverse are similar to the epoxy.

Table 5. Young's Moduli and Poisson's Ratios for
superconducting coil materials

YOUNG'S MODULI 10^4 MN/m² (10^6 psi)

Specimen	Temperature, Kelvin		
	293	77	4
Radial #1 (E ₂₂)	2.82 (4.10)	3.82 (5.53)	4.15 (6.01)
Radial #2 (E ₂₂)	2.68 (3.89)	3.75 (5.43)	4.08 (5.91)
Long. #1 (E ₁₁)	7.72 (11.21)	8.26 (11.97)	8.74 (12.67)
Long. #3 (E ₁₁)	7.39 (10.72)	7.89 (11.44)	8.31 (12.05)
F. E. #1 (E ₁₁)	2.82 (4.10)	3.33 (4.82)	3.56 (5.16)

POISSON'S RATIOS

Specimen	Temperature, Kelvin		
	293	77	4
Radial #1 (ν_{21})	0.146	0.202	0.196
Radial #2 (ν_{21})	0.199	0.248	0.256
Long. #3 (ν_{13})	0.333	0.352	0.352
F. E. #1 (ν_{13})	0.149	0.209	0.221

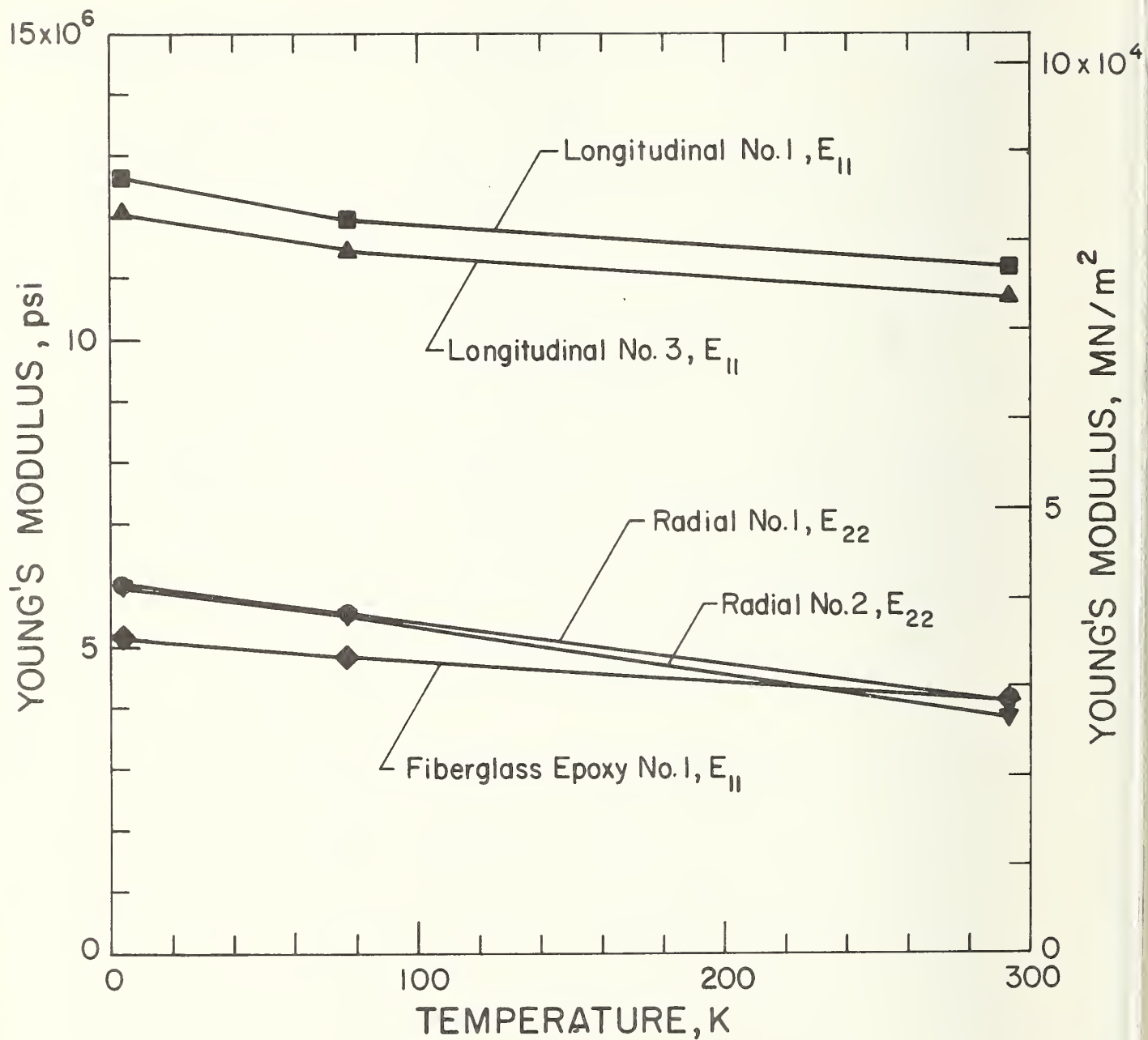


Figure 14. Young's modulus versus temperature for superconducting coil materials.

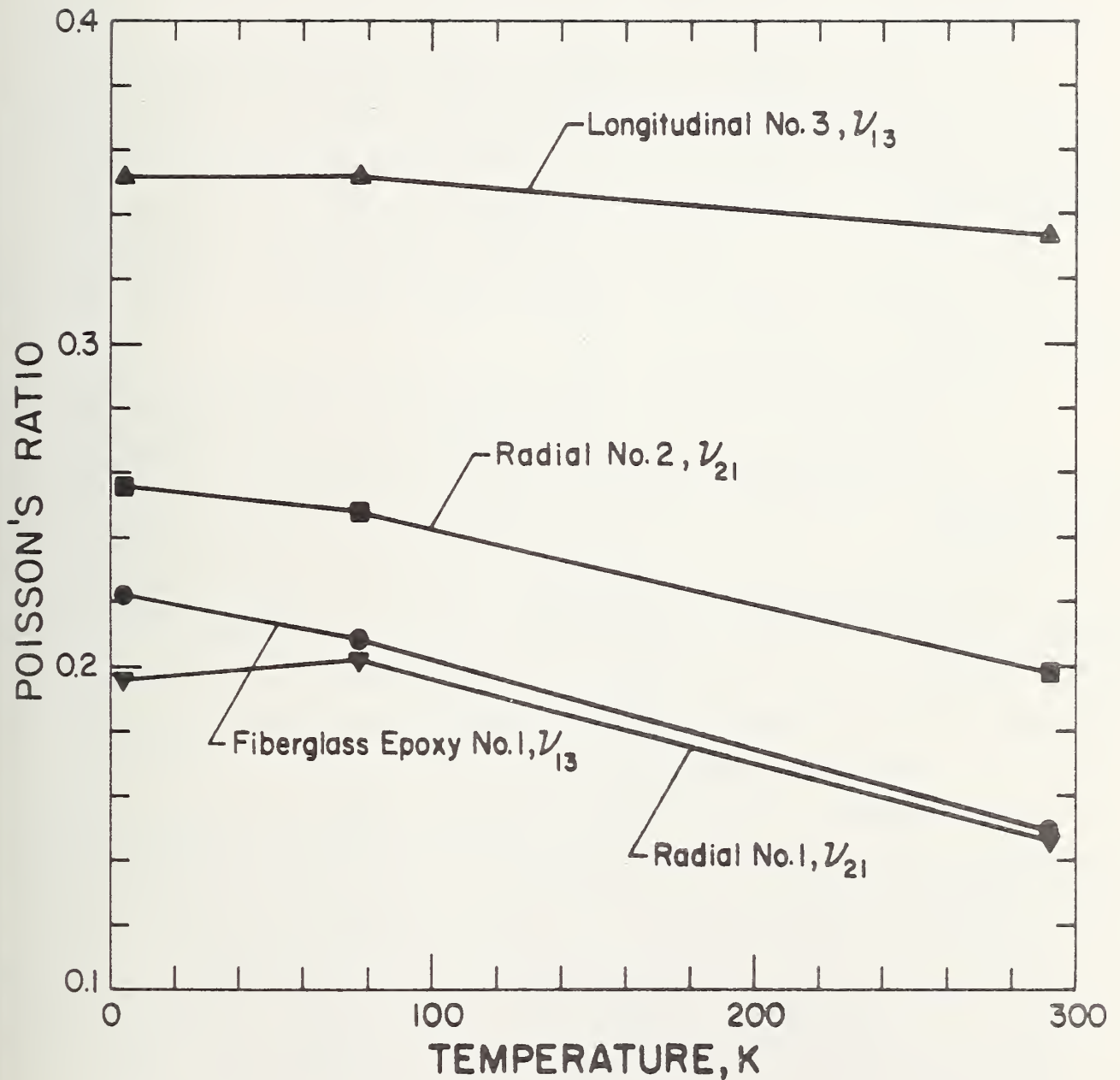


Figure 15. Poisson's ratio versus temperature for superconducting coil materials.

7. PREDICTED VERSUS MEASURED PROPERTIES

The micromechanical laws discussed in previous sections were evaluated using available, appropriate volume fractions and constituent properties. These predicted results are compared with measured room temperature properties in Table 6. The predicted value preferred on a theoretical basis is underlined.

The predicted value of E_{11} was approximately 13% below the measured value. This was probably due to the value of E_f used for the wires as well as to the fact that the contribution of the fiberglass was ignored. The tensile test of the wire showed an increase in E_f with increasing stress (a behavior typical of a stranded specimen). Since the coil is fabricated with considerable tension in the conductor this tension may slightly alter the mechanical properties of the wire.

The predicted values for ν_{13} were about 5% below the measured value. Due to the complexity of the transverse geometry and the fact that ν_f for the wire was assumed to be the same as copper, this agreement is probably fortuitous.

The predicted value of ν_{31} was 0.11. The measured value of ν_{21} was between 0.146 and 0.199. If the material were truly transversely isotropic in the 2 - 3 plane then $\nu_{31} = \nu_{21}$. The discrepancy in these values probably reflects a lack of isotropy which must exist in the 2 - 3 plane. This also is being experimentally measured.

The transverse modulus, E_{22} , is difficult to predict due to the complex stress distribution and to the fact that the transverse properties of fibers or wires are generally not known. The usual procedure is to assume that the transverse fiber properties are equal to the longitudinal properties. The lower bound is given by the series model or equation (12). The most accurate values are produced by the elasticity solutions of Adams [11,14], which bracket the experimental values. The value of E_{22} for the nominal volume fraction of 0.73 is approximately 8% higher than the average measured value.

The predictions of shear modulus G_{13} , vary between 3.45×10^3 MN/m² (0.5×10^6 psi) and 9.16×10^3 MN/m² (1.33×10^6 psi) for four different

Table 6. Room temperature properties of the superconducting coil composite, calculated values and measured values.

Property	Model or Author (Ref.)	Equation Number	V_f	Calculated Values	Experimental Values	Notes
E_{11}	Parallel	[8]	0.73	6.66 (9.66) ^a	7.39 (10.72) ^a 7.72 (11.21) ^a	With $E_f = 11.64 \times 10^6$ psi and neglecting fiberglass
ν_{13}	Parallel	[14] [14]	0.73 0.803	0.319 <u>0.324</u>	0.333	With $\nu_f = 0.33$ and using volume fraction corresponding to 3 direction.
	Rosen (20)	[15]	0.73 0.803	0.320 <u>0.324</u>		
ν_{31}	Calcote (7)	[7]	N. A.	0.11	0.146 - 0.199*	*Experimental values actually ν_{21} and assuming transverse isotropy.
ν_{23}	Adv. Comp. Design Guide (11)	[16]	0.65 0.73 0.803	0.355 0.349 <u>0.335</u>	To be measured	
E_{22}	Series (lower bound)	[9]	0.73 0.65	1.12 (1.67) ^a 0.90 (1.30) ^a	2.82 (4.10) ^a 2.68 (3.89) ^a	The transverse modulus of the wire is assumed equal to the measured longitudinal modulus.
	Adams (et al.) (14)		0.73 0.65	2.97 (4.32) ^a <u>1.96 (2.85)^a</u>		
G_{13}	Adams (et al.) (14)		0.65 0.73	0.630 (0.914) ^a 0.916 (1.33) ^a	To be measured	The shear modulus of the wire was determined from the measured longitudinal modulus and the assumed $\nu = 0.33$ by $G = E/2(1+\nu)$.
	Ekvall (19)	[18]	0.65	0.346 (0.502) ^a		
			0.73	0.433 (0.629) ^a		
			0.803	0.564 (0.818) ^a		
Rosen (20)	[19] [20] [21]	0.73 0.73 0.73	0.545 (0.791) ^a 0.443 (0.643) ^a 0.660 (0.958) ^a			
Foye (22)	[22]	0.73	0.544 (0.789) ^a			
k_{11}	Parallel	[12]	0.73	282 W/mK (163 Btu/hr ft°F)	To be measured	Constituent properties assumed are shown in Table 1.
k_{22}	Series	[13]	0.65	9.95 W/mK (5.75 Btu/hr ft°F)	To be measured	
α_{11}	Parallel	[10]	0.73	$14.2 \times 10^{-6}/K$ ($7.91 \times 10^{-6}/°F$)	$14.0 \times 10^{-6}/K$ ($7.78 \times 10^{-6}/°F$)	
α_{22}	Series	[11]	0.65	$27.25 \times 10^{-6}/K$ ($15.14 \times 10^{-6}/°F$)	$22.9 \times 10^{-6}/K$ ($12.7 \times 10^{-6}/°F$)	Volume fraction of 0.83 was computed assuming a series of rectangles spaced as shown in schematic of coil cross section Fig. 3.
			0.83	<u>$21.96 \times 10^{-6}/K$</u> ($12.20 \times 10^{-6}/°F$)		

^aUnits of 10^4 MN/m² (10^6 psi).

micromechanical solutions as well as a range of representative volume fractions. Since the shear modulus of the wire is not known these values must be considered tentative approximations until the composite shear modulus is measured.

The simple series and parallel models were used along with the appropriate volume fractions to predict the linear coefficients of thermal expansion at room temperature. The agreement between predicted and measured values is within a few percent for both the longitudinal and transverse specimens. Since the actual constituent properties were unknown, nominal values for copper and epoxy were used in the equations. Because of these approximations the close agreement is surprising and perhaps fortuitous.

The general agreement of measured properties and properties predicted by micromechanical methods indicates that these laws can be used to generate composite coil properties sufficiently accurate for preliminary design purposes. Experimental values should be obtained whenever feasible, especially at room temperature. The change of coil composite mechanical properties with temperature can probably be extrapolated very accurately by noting the change with temperature of the major constituent.

7.1 Preliminary Coil Values

By combining the measured properties and the theoretically predicted properties, a set of constitutive relationships for this superconducting coil composite can be established. These properties should be considered as tentative until additional measurements are completed. They are, however, accurate enough for some practical analyses and may actually introduce less error than the analytical model or solution method itself.

The experimental values as well as the calculated values for the properties are average or best values in our judgement. The calculated values are noted by an asterisk. We assume

$$E_{11} = 7.58 \times 10^4 \text{ N/m}^2 = (11 \times 10^6 \text{ psi})$$

$$E_{22} = 2.76 \times 10^4 \text{ N/m}^2 = (4 \times 10^6 \text{ psi})$$

$$\nu_{13} = 0.333$$

$$\nu_{23} = 0.335^*$$

$$G_{13} = 0.69 \times 10^4 \text{ N/m}^2^* = (1 \times 10^6 \text{ psi})^*$$

Substituting these into the compliance matrix, Equation 7, yields

$$10^6 S_{ij} \text{ (N/m}^2\text{)} = \begin{matrix} & \begin{matrix} 13.18 & -12.07 & -12.07 & 0 & 0 & 0 \end{matrix} \\ \begin{matrix} -12.07 \\ -12.07 \\ -12.07 \\ 0 \\ 0 \end{matrix} & \begin{matrix} 36.25 & -12.14^* & 36.25 & 96.79 & 72.50^* & 0 \\ -12.14^* & 36.25 & 96.79 & 0 & 0 & 0 \\ 36.25 & 96.79 & 0 & 0 & 0 & 72.50^* \\ 96.79 & 0 & 0 & 0 & 72.50^* & 0 \\ 72.50^* & 0 & 0 & 0 & 0 & 72.50^* \end{matrix} \end{matrix} \quad (28)$$

To obtain the equation in English units, in the form

$$10^9 S_{ij} \text{ (psi)} = [\text{matrix}],$$

multiply all elements of the matrix on the right hand side of Equation 28 by 6.895.

The thermal conductivity at room temperature is given by the matrix

$$K_{ij} \text{ (W/mK)} = \begin{matrix} & \begin{matrix} 282^* & 0 & 0 \end{matrix} \\ \begin{matrix} 0 \\ 0 \\ 0 \end{matrix} & \begin{matrix} 9.95^* & 0 & 9.95 \end{matrix} \end{matrix} \quad (29)$$

to obtain $K \text{ (Btu/hr ft } ^\circ\text{F)}$ multiply the given matrix elements by 0.578.

The thermal expansion coefficient at room temperature is given by the matrix

$$10^6 \alpha_{ij} \text{ (K}^{-1}\text{)} = \begin{matrix} & \begin{matrix} 14.0 & 0 & 0 \end{matrix} \\ \begin{matrix} 0 \\ 0 \\ 0 \end{matrix} & \begin{matrix} 22.9 & 0 & 22.9 \end{matrix} \end{matrix} \quad (30)$$

to obtain $10^6 \alpha_{ij} \text{ (} ^\circ\text{F}^{-1}\text{)}$, multiply the given matrix elements by 5/9.

7.2 Effect of Curvature

Since the radial tensile specimen was fabricated from slugs machined from an actual solenoidal coil, some shear is introduced away from the centerline of the specimen due to the curvature of the wires, Figure 16a. A question arises as to the effect of this curvature on the experimental values.

A preliminary calculation indicates that the upper bound on the possible error in the calculated moduli from this effect is no more than 10%, and probably much less. We conclude that this can be neglected in the studies at hand.

8. CONCLUSIONS

(1) Comparison of measured macroscopic coil properties to those predicted from constituent properties by micromechanical analyses is reasonably accurate, giving confidence to our formulation of the measurement program.

(2) The modulus and expansion coefficient parallel to the superconducting wire is best predicted by the micromechanical models of binary materials in parallel, while perpendicular to the wire the best predictions come from the series model.

(3) Measurements of the shear moduli and Poisson's ratios are incomplete at this time.

(4) The anisotropy of the material properties is very real, and of such magnitude as to have a strong effect on the stresses on the coil body as a function of operating conditions.

Work is continuing on the following topics

(1) Shear moduli, Poisson's ratios, and thermal conductivity of coil materials.

(2) Moduli, conductivity, and thermal expansion of the superconducting wire.

(3) Analysis of internal strains in the coil structure as a function of winding tension and anisotropic thermal contraction.

(4) Instrumentation procedures on a coil to further test and confirm our experimental and analytical work.

9. ACKNOWLEDGEMENTS

The authors are indebted to M. J. Superczynski of the Annapolis Laboratory - Naval Ship Research and Development Center for providing specimens, the general description of the coil and its manufacturers, and helpful discussions. R. J. Trapani performed several of the calculations for which we are thankful. The critical reading of the manuscript by V. D. Arp is greatly appreciated.

REFERENCES

1. Timoshenko, S. P. and Goodier, J. N., Theory of Elasticity Third Edition, McGraw-Hill Book Company, New York (1970), pp 433-484.
2. Frederick, D. and Chang, T. S., Continuum Mechanics Allyn and Bacon, Inc., Boston, (1965), pp 166-172.
3. Lekhnitskii, S. G., Theory of Elasticity of an Anisotropic Elastic Body, translated from Russian by P. Fern, Holden Day, San Francisco (1963).
4. Hearmon, R. F. S., An Introduction to Applied Anisotropic Elasticity, Oxford University Press, New York (1961).
5. "Element Methods in Stress Analysis", TAPIR, The Technical University of Norway, Trondheim, Norway (1970).
6. Zienkiewicz, O. C. and Cheung, Y. K., The Finite Element Method in Structural and Continuum Mechanics, McGraw-Hill, London, (1967), pp 148-191.
7. Calcote, L. R., Introduction to Continuum Mechanics, D. Van Nostrand Company, New York (1968), pp 67-76.
8. Landau, L. D. and Lifshitz, E. M., Theory of Elasticity, Translation by Sykes, J. B. and Reid, W. H., Pergamon Press, Reading, Mass. (1959), pp 14-17.
9. Carslaw, H. S. and Jaeger, J. C., Conduction of Heat in Solids, second edition, Oxford at the Clarendon Press (1959), pp 38.
10. Calcote, L. R., The Analysis of Laminated Composite Structures, Van Nostrand Reinhold, New York (1969).
11. Advanced Composites Design Guide, Volume 11, Analysis, Air Force Materials Laboratory (AFML/LC), Wright-Patterson Air Force Base, Ohio 45433 (January 1973).
12. Modern Composite Materials, ed. Broutman, L. J. and Krock, R. H., Addison-Wesley Publishing Company, Reading, Mass. (1967).
13. Paul, B., "Prediction of Elastic Constants of Multiphase Materials", Transactions AIME 218, 36-44 (1960).
14. Adams, D. F. and Doner, D. R., "Transverse Normal Loading of a Unidirectional Composite", J. Composite Materials 1, 152 (1967).
15. Chen, C. H. and Cheng, S., "Mechanical Properties of Fiber Reinforced Composites", J. Composite Materials 1, 30 (1967).
16. Whitney, J. M. and Riley, M. B., "Elastic Properties of Fiber-Reinforced Composite Materials", AIAA Journal 4, 1537-1542 (September 1966).
17. Davis, L. W. and Bradstreet, S. W., "Control of Thermal Expansion Through Composite Design", Ceramic Bulletin 50, No. 12 (1971).
18. Schneider, P. J., Conduction Heat Transfer, Addison-Wesley, Cambridge, Mass. (1957) pp 21-26.
19. Ekvall, J. C., "Elastic Properties of Orthotropic Monofilament Laminates", ASME Paper 61-AV-56, presented at Aviation Conference, Los Angeles, California (March 12-16, 1961).

20. Rosen, B. W., Dow, N. F., and Hashin, Z., "Mechanical Properties of Fibrous Composites", NASA CR-31 (April 1964).
21. Hashin, Z. and Rosen, B. W., "The Elastic Moduli of Fiber-Reinforced Materials", Paper No. 63-WA-175, J. Appl. Mech., ASME (June 1964).
22. Foye, R. L., "Advanced Design Concepts for Advanced Composite Airframes", AFML-TR-68-91, Vol. 1 (July 1968).
23. Clark, A. F., Cryogenics 8, 282 (1968).
24. Sparks, L. L., Powell, R. L. and Hall, W. J., "Reference Tables for Low-Temperature Thermocouples", NBS Monograph 124 (June 1972).
25. Automation Industries, Inc., "Technical Data 10-701", (1969).
26. Corruccini, R. J. and Gniewek, J. J., "Thermal Expansion of Technical Solids at Low Temperatures", NBS Monograph 29, (1961).

U.S. DEPT. OF COMM. BIBLIOGRAPHIC DATA SHEET	1. PUBLICATION OR REPORT NO. NBSIR 73-349	2. Gov't Accession No.	3. Recipient's Accession No.
4. TITLE AND SUBTITLE CHARACTERIZATION OF A SUPERCONDUCTING COIL COMPOSITE		5. Publication Date December 1973	6. Performing Organization Code
		7. AUTHOR(S) C.W. Fowlkes, P.E. Angerhofer, R.N. Newton & A.F. Clark	
9. PERFORMING ORGANIZATION NAME AND ADDRESS NATIONAL BUREAU OF STANDARDS DEPARTMENT OF COMMERCE Washington, D.C. 20234		10. Project/Task/Work Unit No. 2750538	11. Contract/Grant No.
		12. Sponsoring Organization Name and Address Annapolis Laboratory Naval Ship Research and Development Center Annapolis, Maryland 21402	
14. Sponsoring Agency Code			
15. SUPPLEMENTARY NOTES			
<p>16. ABSTRACT (A 200-word or less factual summary of most significant information. If document includes a significant bibliography or literature survey, mention it here.)</p> <p>The superconducting coil composite material being utilized by the Annapolis Laboratory of the Naval Ship Research and Development Center is characterized by its mechanical and thermal properties. The Young's moduli, Poisson's ratios, and thermal contractions are measured from room temperature to 4 K and reported in this interim report. A micro-mechanical analysis based upon volume fractions of constituents is used to predict room-temperature properties, and a comparison is made to the measured values.</p>			
<p>17. KEY WORDS (Alphabetical order, separated by semicolons)</p> <p>Composite; low temperature; Poisson's ratio; superconductor; thermal expansion; Young's modulus.</p>			
<p>18. AVAILABILITY STATEMENT</p> <p><input checked="" type="checkbox"/> UNLIMITED.</p> <p><input type="checkbox"/> FOR OFFICIAL DISTRIBUTION. DO NOT RELEASE TO NTIS.</p>		<p>19. SECURITY CLASS (THIS REPORT)</p> <p>UNCL ASSIFIED</p>	<p>21. NO. OF PAGES</p>
		<p>20. SECURITY CLASS (THIS PAGE)</p> <p>UNCL ASSIFIED</p>	<p>22. Price</p>